MNRAS **000**, 1–13 (2017) Preprint 29 October 2022 Compiled using MNRAS LATEX style file v3.0

How *Cassini* Can Constrain Tidal Dissipation in Saturn

Jing Luan,[1⋆] Jim Fuller,[2,3] Eliot Quataert[1]
[1] *Astronomy Department, University of California at Berkeley, Berkeley, CA 94720, US*
[2] *Kavli Institute for Theoretical Physics, Kohn Hall, University of California, Santa Barbara, CA 93106, USA*
[3] *TAPIR, Walter Burke Institute for Theoretical Physics, Mailcode 350-17, Caltech, Pasadena, CA 91125, USA*

Accepted XXX. Received YYY; in original form ZZZ

arXiv:1707.02519v1 [astro-ph.EP] 9 Jul 2017

ABSTRACT
Tidal dissipation inside giant planets is important for the orbital evolution of their natural satellites. It is conventionally treated by parameterized equilibrium tidal theory, in which the tidal torque declines rapidly with distance, and orbital expansion was faster in the past. However, Lainey et al. (2017) find that some Saturnian satellites are currently migrating outward faster than predicted by equilibrium tidal theory. Resonance locking between satellites and internal oscillations of Saturn, proposed by Fuller et al. (2016), naturally matches the observed migration rates. Here, we show that the resonance locking theory predicts dynamical tidal perturbations to Saturn's gravitational field in addition to those produced by equilibrium tidal bulges. We show that these perturbations can likely be detected during *Cassini*'s proximal orbits if migration of satellites results from resonant gravity modes, but will likely be undetectable if migration results from inertial wave attractors or dissipation of the equilibrium tide. Additionally, we show that the detection of gravity modes would place constraints on the size of the hypothetical stably stratified region in Saturn.

Key words: planets and satellites: interiors – planets and satellites: physical evolution – hydrodynamics – waves

1 INTRODUCTION

Some of the Saturnian satellites are believed to have migrated outward due to tidal interaction with Saturn (Peale 1999, and reference therein). The tidal origin of their migration was first proposed by Goldreich (1965). Tidal interaction is conventionally treated assuming that equilibrium tides are dissipated by a fraction, $1/Q$, every cycle[1]. This approximation originates from studies of terrestrial bodies in the solar system (e.g. Jeffreys 1952). The frequencies of free oscillations of small solid bodies are much higher than that of tidal forcing in most cases, and therefore their instantaneous tidal deformation is well approximated by the equilibrium tide. However, caution should be taken when extending this theory to gaseous planets, because they are larger and less dense and thus they may support free oscillation modes or waves whose frequencies match those of tidal forcing. The conventional treatment, i.e., dissipation of the equilibrium tide with Q independent of time, is so convenient that it is widely applied to both planets and stars. The resulting tidal torque decreases by the sixth power of distance (e.g. Murray & Dermott 1999). Consequently, a conceptual belief has been established over years that tidal interaction weakens rapidly with distance, and that most of the satellite's orbital expansion took place in the distant past when the satellites were closer to Saturn.

However, Lainey et al. (2017) recently reported surprisingly fast ongoing migration for Enceladus, Tethys, Dione, and Rhea. This observation disfavors the conventional belief of equlibrium tidal dissipation. Instead, Fuller et al. (2016) propose that satellites enter resonance locks with internal oscillations of Saturn. The planet's oscillation frequencies and satellite orbital frequencies evolve together such that resonances can be maintained over long time scales. Fuller et al. (2016) predict orbital migration rates consistent with observations, assuming that the oscillation frequencies evolve on the thermal timescale of Saturn. In this scenario, the migration of satellites is controlled by the evolution of Saturn's interior, which is independent of the distance of the satellites from Saturn. The satellite distance does affect capture or breaking of resonance locks, which will be described qualitatively below but is not the focus of this paper.

Resonance locking, first introduced into astronomy by Witte & Savonije (1999), is similar to surfing. A surfer slides sideways on a wavefront, gaining just the right amount of speed to move together with it. A surfer and ocean wave are analogous to a satellite and Saturnian oscillation. The

⋆ E-mail: jingluan@berkeley.edu
[1] A cycle could be one orbit period of satellite or one rotation period of planet or some combination of them, depending the specific case.

© 2017 The Authors

essential difference is that a satellite excites the oscillation of Saturn, whereas an ocean wave propagates independently of a surfer. It seems to violate energy conservation that a satellite gains energy and angular momentum from an oscillation it excites, but it does not. Because Saturn rotates faster than a satellite orbit, the oscillation of Saturn propagates prograde with the satellite in the inertial frame, but retrograde relative to the frame co-rotating with Saturn at angular frequency Ω_S. In the inertial frame, Saturn contains less energy and angular momentum in the presence of the oscillation than in its absence (Pierce 1974). Therefore, the oscillation excited by the satellite contains negative energy and angular momentum, whereas the satellite gains positive energy and angular momentum that originates from the rotation of Saturn, and the oscillation of Saturn is merely an intermediary.

However, capture into a resonance lock is not guaranteed. Consider the case in which the interior evolution of Saturn pushes an oscillation towards resonance with a satellite. The oscillation gets excited by the tidal force of the satellite, but it also gets damped through dissipative processes, e.g., heat diffusion and turbulent viscosity. The damping produces a phase lag between the satellite and the oscillation of Saturn, leading to a positive torque on the satellite. The tidal torque is proportional to the phase lag and the energy of the oscillation. The former is $\propto \gamma$, the damping rate of oscillation, and the latter is $\propto A^2$, where A is the amplitude of the oscillation. The tidal torque, $T_{\rm osc} \propto \gamma A^2$, grows near resonance[2]. The resonance lock will succeed if the tidal torque becomes large enough for the satellite to evolve at the same rate as the oscillation in the frequency domain. Otherwise, the oscillation sweeps past the satellite in the frequency domain, torquing it temporarily, but failing to lock it.

The tidal torque can grow near resonance through two mechanisms. A resonance with a gravity mode (g-mode) increases A but keeps γ constant. G-modes can exist if stable stratification is present inside Saturn. An inertial wave attractor, in contrast, increases γ but keeps A constant. Hence, to produce the same torque on a satellite, the two mechanisms perturb the external gravity field differently. The potential perturbation has dependence $\Phi' \propto A$ but is almost independent of γ [3]. Therefore, a resonant gravity mode or inertial wave attractor are distinguishable from a gravity measurement. The *Cassini* spacecraft, currently in its proximal orbits, will fly by the surface of Saturn 22 times by September 2017 (Dunford et al. 2017). Ten of those close encounters are dedicated to measure the gravitational field of Saturn [4]. The anticipated accuracy is unprecedented,[5] and may allow us to distinguish between a resonant g mode and an inertial wave attractor, or at least constrain their parameters.

This paper is arranged as follows. Section 2 describes how a g mode and an inertial wave attractor work in a resonance lock. Section 3 comments on the influence of orbital mean motion resonances (MMRs) on resonance locks, because most of Saturn's major satellites are involved in MMRs. We estimate perturbations to the gravitational potential of Saturn by a g mode and an inertial wave attractor in Section 4. Section 5 compares our results with the expected accuracy of the gravity measurement by *Cassini*. Section 6 estimates the gravitational potential due to the fundamental modes of Saturn which are proposed to excite the observed density waves in the C ring (Hedman & Nicholson 2013). We find it far below the anticipated detection threshold of *Cassini*. In Section 7, we discuss our results and present our conclusions. Readers mainly interested in indications for observation are suggested to read through Section 2 to get the basic idea of resonance locking and then focus on Section 5.

2 CANDIDATES FOR RESONANCE LOCK

In this section, we discuss two different ways resonance locking operates, assuming successful locking in each case.

2.1 Gravity modes

A gravity mode propagates only in stably stratified regions in which buoyancy is able to restore oscillations (e.g. Cox 1980). Seismology of Saturn's ring system reveals fundamental modesin Saturn (Hedman & Nicholson 2013). Fine splitting of those fundamental modes indicates the existence of stable stratification inside Saturn (Fuller 2014).

The amplitude of a gravity mode grows as its frequency converges with the tidal forcing frequency of a satellite. It is instructive to visualize the propagation cavity of a g mode as a spring, and tidal force of the satellite swings the outer end of the 'spring'.[6] The excited oscillatory motion then propagates inward, which is essentially an ingoing g wave. It gets reflected at the inner boundary of the propagation cavity, and returns to the outer boundary, forming an outgoing g wave. Ingoing and outgoing g waves with the right relative phase compose a standing g wave, i.e., a g mode. Consider a g mode with n_r radial nodes and angular frequency σ_g. The phase of the g wave increases by $2\pi n_r$ as it returns to the outer boundary after one reflection. Meanwhile, the tidal force changes its phase by $2\pi n_r \sigma/\sigma_g = 2\pi n_r(1+\delta\sigma/\sigma_g)$, where $\sigma = \sigma_g + \delta\sigma$ is the angular frequency of the tidal forcing. As long as the frequency mismatch, $|\delta\sigma| \ll \sigma$, the wave remains nearly in phase with tidal force, so its amplitude increases. The amplitude grows by roughly the same amount every time the wave returns to the outer boundary. After $\sim 1/|\delta\sigma|$, the wave shifts out of phase with respect to

[2] The growth rate of the mode energy, $d(A^2)/dt$, also contributes to $T_{\rm osc}$. It needs to be taken into account if we consider the capture probability of the resonance lock, which is not the topic of this paper. Here, we assume the system is in resonance lock. It is in an equilibrium state (stable fixed point) and A hardly changes.
[3] The dissipation rate, γ, determines the phase lag of the oscillation pattern and therefore also determines the phase of Φ'. But the phase lag itself is probably too tiny to measure.
[4] *Cassini* sends radio signals at certain wavelengths back to earth. Its velocity along the line of sight is measured through Doppler shifts. Its acceleration is then extracted from the velocity as a function of time.

[5] Through private communication with Phillip D. Nicholson.
[6] The tidal force of the satellite operates everywhere, but it is strongest at the outer end of the propagation cavity, because tidal gravity potential is $\propto (r/a)^l$ (e.g. Murray & Dermott 1999).

the tidal force, and its amplitude saturates. The saturation amplitude is $A_{\rm sat} \propto 1/|\delta\sigma|$.

As a g mode frequency converges with the tidal forcing frequency, $|\delta\sigma|$ decreases. In the case of slow convergence, which applies to Saturn, a g mode has enough time to reach $A_{\rm sat}$ at any given instant. Therefore, the amplitude of a g mode, $A \sim A_{\rm sat} \propto 1/|\delta\sigma|$, increases upon resonance. The essential reason is that the g mode has a well defined propagation cavity such that it returns to where it gets excited after having accumulated an integer multiple of 2π in phase. We will see that inertial waves do not share this property and therefore their amplitude does not grow upon resonance.

On the other hand, the damping rate, γ, remains the same as long as a g mode stays within the linear regime, i.e. $\xi_r k_r \ll 1$. Turbulent viscosity in convective regions and heat diffusion in stably stratified regions both damp g modes. They are estimated in Appendix A to be

$$\gamma_{\rm turb} \sim \frac{0.1 \sim 1}{(n_r+1)}\,{\rm Gy}^{-1}\,, \tag{1}$$

and

$$\gamma_{\rm diff} \sim (0.1 \sim 1)(n_r+1)\,{\rm Gy}^{-1}\,, \tag{2}$$

which are both small. Turbulent viscosity is weak because convection in Saturn turns over on a timescale much longer than the typical oscillation period, $\sim \Omega_S^{-1}$. Therefore eddies as large as the local scale height do not act like viscosity (Goldreich & Nicholson 1977). Eddies turning over on a timescale similar to or shorter than the oscillation period are downward in the turbulent cascade. They are small and slow, and for a Kolmogorov cascade, they have velocity, $v \propto l^{1/3}$, where l here refers to the linear size of eddy. Turbulent viscosity is weak because kinetic viscosity is roughly the length multiplied by the velocity of the eddy. Damping by heat diffusion is weak as well, mainly because the current thermal timescale of Saturn is long. Note that $\gamma_{\rm diff}$ is independent of the specific mechanism for heat diffusion, as demonstrated in Appendix A2. It could be created by diffusion through radiation or conductivity.

We acknowledge that γ for g modes is very uncertain. There may exist other damping mechanisms beyond our knowledge, e.g. damping through conversion to inertial waves, which we briefly discuss in Section 5. Fortunately, as we will see in Section 5, our main results depend on γ weakly.

2.2 Inertial wave attractors

Inertial waves are restored by the Coriolis force, $-2\boldsymbol{\Omega_S} \times \dot{\boldsymbol{\xi}}$, and therefore they reside in rotating bodies within the frequency range $-2\Omega_S < \sigma < 2\Omega_S$ (Greenspan 1968).[7] The WKB dispersion relation is

$$\sigma = \frac{|2\boldsymbol{\Omega_S}\cdot\mathbf{k}|}{k}\,, \tag{3}$$

i.e., the angle β between the spin axis and the wave vector satisfies $\cos\beta = \pm\sigma/(2\Omega_S)$. Therefore, reflection of inertial wave rays is nonspecular except when the reflection plane is perpendicular to the spin axis. Nonspecular reflection prevents inertial waves from returning to where they are excited, and thus, unlike g modes, the amplitudes of inertial waves do not grow. This heuristic is not exact but serves an intuitive way for understanding inertial waves. Strict mathematical development is found in Ogilvie (2013), which we will briefly review in Section 5.

Inertial waves do not form standing waves as normally defined (Greenspan 1968), and therefore they are usually not referred to as inertial modes. However, at certain frequencies, after multiple reflections inertial wave rays converge toward a spatial pattern called a wave attractor (e.g. Maas et al. 1997). An inertial wave attractor closes in space, and therefore is analogous to a mode. However, a mode is identified by quantum numbers, namely the numbers of radial and angular nodes, whereas wave attractors may not be quantized in a similar way.

Inertial wave attractors usually form at discrete frequencies, at which the damping of inertial waves peaks (e.g. Ogilvie & Lin 2004). Ogilvie (2013) show that smaller kinetic viscosity sharpens wave attractors, making their peaks in tidal dissipation narrower and higher, until nonlinear damping starts to operate. Linear damping scales with the square of the velocity shear multiplied by kinetic viscosity. Nonlinear damping, e.g., shock breaking or generation of turbulence, also contributes to γ if the velocity shear exceeds the linear regime. Either way, inertial wave attractors promote damping, i.e., γ increases as a satellite's tidal forcing frequency approaches the frequency of an inertial wave attractor.

Inertial wave attractors form by multiple reflections. Reflection, or more generally speaking, scattering conserves the total action of a wave, which is the classical physics analogue to the number of quanta in quantum physics. The total energy of an inertial wave is proportional to the action multiplied by σ. It follows that A is conserved by reflection, since the total wave energy is $\propto A^2$. Therefore, the formation of inertial wave attractors does not change A.

Since the tidal torque scales as $T_{\rm osc} \propto \gamma A^2$, the torque on a satellite increases as it approaches an inertial wave attractor in the frequency domain. However, the physical mechanism underlying resonance locking differs between an inertial wave attractor and a g mode. To summarize, a g mode increases A while keeping γ constant, whereas an inertial wave attractor increases γ while keeping A constant.

3 MEAN MOTION RESONANCE

Saturn has three pairs of satellites involved in orbital MMRs (e.g. Murray & Dermott 1999), in which mutual interaction fixes the orbital period ratios of the satellites. The MMRs are Mimas-Tethys in a 4 : 2 inclination MMR, Enceladus-Dione in a 2 : 1 eccentricity MMR, and Titan-Hyperion in a 5 : 3 eccentricity MMR (Urban & Seidelmann 2012). Both satellites in each pair must share the same long-term migration rate $\langle \dot{a}/a \rangle$, i.e., the migration rate averaged over billion year timescales.

Lainey et al. (2017) report a migration rate, $\dot{a}/a \sim 1/(5\,{\rm Gyr})$, for Enceladus, Tethys, Dione and Rhea. Data sets with time spans of $\sim 100\,{\rm yr}$ and $\sim 20\,{\rm yr}$ are analyzed independently, producing consistent results. Mimas had been re-

[7] For tidally excited oscillations this condition is satisfied as long as the azimuthal order of the oscillation mode, m, is less than or equal to two.

ported to migrate inward by Lainey et al. (2012). However, it should migrate outward together with its MMR companion, Tethys. Luan & Goldreich (2017) speculate that the inward migration of Mimas may be biased by the MMR torque which overwhelms the migration torque by a factor of $\sim 10^5$ and librates every $\sim 80\,$yr. The data set spanning over $\sim 100\,$yr employed by Lainey et al. (2012) most likely does not completely average out the MMR torque. There are not yet published migration rates for Titan or Hyperion.

Convergent migration is necessary for MMR capture. Assuming both satellites migrate due to resonance locking before they get caught in a MMR, the corresponding oscillations of Saturn must evolve convergently in the frequency domain. However, this requirement is not naturally satisfied by resonance locking, but instead depends on the evolution of the interior of Saturn, of which we lack enough understanding to accurately assess.

The outer satellite in a MMR is likely no longer in a resonance lock with Saturn. Once captured in a MMR, the satellite migrates in the frequency domain at the same rate as the inner satellite, rather than the oscillation of Saturn locking it in the past. Therefore, a resonance lock is broken by the formation of a MMR. It follows that Tethys, Dione and Hyperion are not currently in a resonance lock with an oscillation of Saturn. In addition, to maintain a MMR, the inner satellite must provide the outer satellite with angular momentum, which originates from the tidal torque by a resonance lock with Saturn. Therefore, a MMR must increase the amplitude of a resonantly locked g mode, or the damping rate of a resonant inertial mode attractor.

An oscillation of Saturn, and the inner and outer satellites form a resonance chain. The planet and inner satellite are linked by a resonance lock, while the inner and outer satellites are linked by a MMR. All three must evolve together in the frequency domain. Hence, an oscillation of Saturn produces a torque on a satellite through a resonance lock,

$$T_{\rm mig} = \frac{1}{2} m_s (G M_S a)^{1/2} \left(\frac{\dot{a}}{a}\right) \times \begin{cases} 1 + \frac{m_{\rm out}}{m_s}\left(\frac{a_{\rm out}}{a}\right)^{1/2}, & \text{inner satellite in MMR}; \\ 0, & \text{outer satellite in MMR}; \\ 1, & \text{satellite not in MMR}, \end{cases} \tag{4}$$

where m_s and a denote the mass and orbital semi-major axis of the satellite in a resonance lock, and $m_{\rm out}$ and $a_{\rm out}$ the mass and orbital semi-major axis of the outer satellite in the MMR.

Although it is not involved in the resonance lock, the outer satellite in the MMR still raises a tidal bulge on Saturn. This is often called the equilibrium tide, although in a neutrally stratified body it is not equivalent to the conventionally defined equilibrium tide, as discussed in Section 4.2. Small co-orbital satellites of Tethys and Dione are used by Lainey et al. (2017) to constrain the gravitational potential created by the tidal bulges induced by Tethys and Dione respectively. They are consistent with what is expected theoretically. Unfortunately, these two satellites are not in a resonance lock with Saturn, since they are both outer satellites in their respective MMRs.

4 GRAVITATIONAL POTENTIAL PERTURBATIONS

An oscillation of Saturn perturbs its external gravitational potential because the density field is perturbed. Even for the same torque provided by a resonance lock, a g mode and inertial wave attractor result in distinct gravitational potentials.

4.1 Gravity modes

We assume stable stratification to reside between radii $r_c < r < r_b$, where r_b is the bottom of the outer convective zone. Fuller (2014) propose a model with $r_c \approx 0.1 R_S$ and $r_b \approx 0.4 R_S$. The angular frequency of a g mode excited by a satellite in the rest frame of Saturn is $\sigma = m(\Omega_S - \Omega_{\rm orb})$, where m is the azimuthal order. Since $\sigma \sim \Omega_S$, the Coriolis force strongly influences the angular pattern of a g mode by restricting horizontal motion[8]. In the traditional approximation, Hough functions, rather than spherical harmonic functions, are the eigenfunctions of the angular part of the equations of motion (e.g. Chapman & Lindzen 1970)[9]. Hough functions are quantized by their angular degree, n[10], and their azimuthal order, m. Modes excited by the tidal potential of a satellite must have their azimuthal order match that of the tidal potential field. The allowed values are $n = m,\ m+2,\ m+4$, etc. The corresponding g modes are closely packed in the frequency domain. In other words, rotation makes the number of g modes per unit frequency larger than in the non-rotating case (refer to Figure 1 in Fuller et al. 2016). One important consequence is that satellites have more chances to encounter g modes in the frequency domain, which is a precondition favoring resonance locking.

Consider a g mode with n_r radial nodes in the stably stratified region. The corresponding gravitational potential perturbation, Φ_g, is dominated by the outermost half wavelength between $r_b - \lambda_1 < r < r_b$, called the first half wavelength. Other half wavelengths partially cancel the potential perturbation generated by the first one but by at most 50%. The evanescent zone, i.e., the outer convective region, has no radial nodes in it. Its contribution to Φ_g has the same sign as that contributed by the first half wavelength, and thus strengthens the latter. These claims are justified in Appendix C. Below we estimate the potential perturbation due to the first half wavelength, Φ_1. We simplify the first half wavelength by collapsing its density perturbation onto

[8] Vertical motion is predominantly controlled by gravity and pressure in stably stratified layers, and thus the Coriolis force is neglected in the radial direction.

[9] We constrain ourselves to Hough function of the first kind. Satellites orbit almost in the equatorial plane of Saturn, favoring excitation of modes concentrated toward the equator. Hough functions of the second kind concentrate toward the poles, as $|\sigma/(2\Omega_S)|$ is close to unity (Longuet-Higgins 1968), which is the case of interest in this paper. Modes with $n = m+1,\ m+3$, etc., are anti-symmetric about Saturn's equator, and therefore are not excited. Modes with $n = -(m+1),\ -(m+2),\ -(m+3),\ -(m+4)$, etc, are Hough functions of the second kind.

[10] Hough functions' n is analogous to l for spherical harmonics.

a layer at r_b. Poisson's equation reduces to

$$\begin{aligned}\nabla^2\Phi_1 &= 4\pi G\rho'(r,\theta,\varphi;t)\\ &= 4\pi G\Sigma_1\delta(r-r_b)\Theta_{nm}(\theta)e^{i(\sigma_m t+m\varphi)}\,, \end{aligned}\quad (5)$$

where ρ' is the Eulerian perturbation of density, Σ_1 is the column density perturbation, θ and φ are the colatitude and longitude in the rest frame of Saturn, $\Theta_{nm}(\theta)$ is the Hough function with azimuthal order, m, and latitudinal degree n, $\delta(r)$ is the Dirac delta function, and

$$\sigma_m \equiv m(\Omega_S - \Omega_{\rm orb})\,. \quad (6)$$

The eigenfunctions of the angular part of the Laplace operator in spherical coordinates are $\bar{P}_{lm}(\cos\theta)\exp(im\varphi)$, where $\bar{P}_{lm}(x)$ is a normalized associated Legendre polynomial. In order to solve for Φ_1, we first project the Hough function, Θ_{nm}, onto $\bar{P}_{lm}$. In this paper, we only consider the case $m=2$, because the leading order of the tidal field of the satellite is its quadrupole with $l=m=2$ (e.g. Murray & Dermott 1999). From now on we omit the index m, unless otherwise mentioned. We expand

$$\Theta_n(\theta) = \sum_{l\geq 2}^{\text{even } l}\mathcal{B}_{nl}\bar{P}_l(\cos\theta)\,, \quad (7)$$

where we adopt the expansion coefficients, $\mathcal{B}_{nl}$, in Table (31) in Flattery (1967). Then the solution for Φ_1 is also represented in the form of an expansion,

$$\Phi_1(r>r_b) = \sum_{l\geq 2}^{\text{even } l}\Phi_{nl}\bar{P}_l(\cos\theta)\exp(i\sigma t+i2\varphi)\,, \quad (8)$$

where

$$\Phi_{nl} \equiv -4\pi G\Sigma_1 r_b\frac{\mathcal{B}_{nl}}{(2l+1)}\left(\frac{r_b}{r}\right)^{l+1}\,. \quad (9)$$

A mode stores the same amount of energy, $E_{\rm node}$, between each pair of consecutive radial nodes. The total energy of a g mode with n_r nodes is $(n_r+1)E_{\rm node}$, assuming that the evanescent region stores energy $\sim E_{\rm node}$. The mode energy gets damped at the rate, $\gamma(n_r+1)E_{\rm node}$. Correspondingly, the negative angular momentum carried by a retrograde mode gets damped at the rate, $\gamma(n_r+1)E_{\rm node}/\omega_p$, where $\omega_p = -\sigma/m = -\Omega_S+\Omega_{\rm orb}\approx -\Omega_S$ is the azimuthal phase speed of the retrograde mode. In the equilibrium state of a resonance lock, i.e., not during capture or breaking of a resonance lock, the mode keeps its energy and angular momentum constant. Thus, the damped negative angular momentum of the mode must be replenished by the satellite. Because angular momentum is an invariant between rotating and inertial frames (Pierce 1974), the satellite gains positive angular momentum at the rate,

$$T_g = -(n_r+1)E_{\rm node}\frac{\gamma}{\omega_p}\approx (n_r+1)E_{\rm node}\frac{\gamma}{\Omega_S}\,. \quad (10)$$

The requisite torque to push a satellite migrating at a rate $\dot{a}/a$ is equation (4).

Equations (8) and (9) express Φ_1 in terms of Σ_1. Equations (10) and (4) relate $E_{\rm node}$ and $\dot{a}/a$. Next, we relate $E_{\rm node}$ and Σ_1, which will enable us to express Φ_1 in terms of $\dot{a}/a$. We constrain ourselves to the most general relations for g modes, making our result least dependent on the specific model of stable stratification in Saturn. There are two reasons for doing so. First, stable stratification is hypothetical; second, the biggest uncertainty in our result is γ for g modes, and thus it is not worth spending much effort on the details of models for stable stratification. Our derivations are based on the following three assumptions:

(i) The Eulerian density perturbation is

$$\rho' \sim \frac{d\rho}{dr}\xi_r\frac{\sigma^2\rho}{k_h^2 p}\,, \quad (11)$$

where $d\rho/dr$ is the gradient of the background density profile, k_h is the horizontal wave number, and ρ and p are the unperturbed background density and pressure. The derivation of ρ' is in appendix B.

(ii) The displacement of a g mode is dominated by its horizontal component,

$$\xi_h \gg \xi_r\,. \quad (12)$$

(iii) The bottom of the outer convective zone is the upper edge of the propagation cavity of a g mode. At this outer turning point, the wavelength of a g mode is comparable to the local scale height, where the WKB dispersion relation starts to break down. For simplicity, we do not distinguish a pressure scale height and a density scale height. Consequently, at r_b,

$$k_r \sim \frac{1}{\lambda_1}\sim\frac{1}{H}\,. \quad (13)$$

The energy in each node of a g mode is then

$$E_{\rm node}\sim r_b^2\lambda_1\rho_b\sigma^2\xi_h^2 \sim r_b^2\rho_b\sigma^2\frac{\xi_r^2 k_r}{k_h^2}\,. \quad (14)$$

The column density perturbation of the first half wavelength is

$$\Sigma_1 \sim \rho'\lambda_1\,, \quad (15)$$

where we have adopted $d\rho/dr\sim\rho_b/H$. Eliminating ξ_r in equations (14) and (15), we obtain

$$\Sigma_1 \sim \frac{r_b^2\lambda_1\xi_r\rho_b\sigma^2}{g_b H^2 K_n} \quad (16)$$

$$\sim \frac{E_{\rm node}^{1/2}\rho_b^{1/2}\sigma}{g_b H^{1/2} n}\,, \quad (17)$$

where g_b is the gravity at r_b, $\bar{\rho}\sim M_S/R_S^3$, and we have expressed the horizontal wavenumber ,

$$k_h = \frac{K_n^{1/2}}{r}\approx\frac{n}{r}\,. \quad (18)$$

This approximation holds true if $4\Omega_S^2/(gk_r)\ll 1$ (Longuet-Higgins 1968). For azimuthal order, $m=2$, n has to be even and ≥ 2, since we only consider Hough functions of the first kind. Combining equations (4), (9), (10) and (17) and eliminating $E_{\rm node}$ and Σ_1, we obtain the gravity anomaly,

$$\begin{aligned}\frac{\Phi_{nl}}{(-GM_S/R_S)} \sim\ & \frac{\mathcal{B}_{nl}}{(2l+1)}\left(\frac{R_S}{a}\right)^2\left(\frac{r_b}{R_S}\right)^{l+2}\left(\frac{R_S}{r}\right)^{l+1}\left(\frac{g_S}{g_b}\right)\\ &\times\left(\frac{\Omega_S}{\Omega_{\rm orb}}\right)^{3/2}\left(\frac{\dot{a}/a}{(n_r+1)\gamma}\right)^{1/2}\left(\frac{m_s}{M_S}\right)^{1/2}\\ &\times\left(\frac{\rho_b}{\bar{\rho}}\right)^{1/2}\left(\frac{R_S}{K_n H}\right)^{1/2}\,,\end{aligned} \quad (19)$$

where $g_S \equiv GM_S/R_S^2$. We have replaced σ by $2\Omega_S$ for azimuthal order of 2 which is the case we consider here. Note that the above expression corresponds to a satellite not in a MMR, e.g., Rhea. The outer satellite in a MMR, such as Tethys and Dione, is not involved in a resonance lock, and thus there is no Φ_{nl}. For the inner satellite in a MMR, namely Mimas, Enceladus and Titan, we need to replace $\dot{a}/a$ by the following factor,

$$\left(\frac{\dot{a}}{a}\right)\left(1+\frac{m_{\rm out}}{m_s}\left(\frac{a_{\rm out}}{a}\right)^{1/2}\right) . \tag{20}$$

The analysis above assumes linear damping. However, at large $k_r\xi_r$, nonlinear damping sets in and limits the amplitude. Different nonlinear effects, e.g. three-mode coupling (e.g. Wu & Goldreich 2001; Weinberg et al. 2012), generation of turbulence (e.g. Hodges 1967), wave front steepening (e.g. Greenspan 1958), etc., could limit $k_r\xi_r$ to different thresholds. However, we do not know which nonlinear effect dominates, without good knowledge of the stratification in Saturn. Without any better criterion, we employ

$$k_r\xi_r|_{r_b} \sim 1 \tag{21}$$

as the threshold over which nonlinear damping would limit the amplitude. Combining equations (4), (10), (13) and (14), we obtain

$$\begin{aligned} k_r\xi_r|_{r_b} \quad \sim \quad & n\left(\frac{\dot{a}/a}{(n_r+1)\gamma}\right)^{1/2}\left(\frac{m_s}{M_S}\right)^{1/2}\left(\frac{\Omega_{\rm orb}}{\Omega_S}\right)^{1/2} \\ & \times\left(\frac{R_S}{H}\right)^{1/2}\left(\frac{R_S}{r_b}\right)^2\left(\frac{a}{R_S}\right)\left(\frac{\bar{\rho}}{\rho_b}\right)^{1/2} . \end{aligned} \tag{22}$$

Similarly, for inner satellites in a MMR, $\dot{a}/a$ should be replaced by equation (20).

4.2 Inertial wave attractors

This subsection mainly quotes Section 4 in Ogilvie (2013)[11], which studies slow oscillations in slowly rotating barotropic bodies with $\sigma < 2\Omega_S \ll (GM_S/R_S^3)^{1/2}$. A barotropic fluid has its pressure uniquely related to density and therefore is neutrally stratified. These conditions apply for inertial waves in the outer convective region of Saturn. The wave displacement is decomposed into a non-wave-like part, $\boldsymbol{\xi}_{\rm nw}$, and a wave-like part, $\boldsymbol{\xi}_{\rm w}$. The former is the instantaneous hydrostatic response of the fluid to the external tidal force from the satellite, while the latter is driven by the unbalanced Coriolis force induced by the former, $-2\boldsymbol{\Omega_S}\times\dot{\boldsymbol{\xi}}_{\rm nw}$. Note that the instantaneous hydrostatic response, $\boldsymbol{\xi}_{\rm nw}$, is conceptually similar but not equivalent to the conventional equilibrium tide. The equilibrium tide represents the tidal response in the zero frequency limit and is not well defined in the absence of stable stratification. Since Saturn is believed to be mostly convective, the non-wave-like hydrostatic response instead of the equilibrium tide is the proper term here, although sometimes people do not distinguish them.

The non-wave like part, $\boldsymbol{\xi}_{\rm nw}$, generates a gravitational potential proportional to that of the satellite,

$$\begin{aligned} \Phi_{\rm nw}(r>R_S) \quad = \quad & \sum_{l,m} k_{lm}\Psi_{lm}\left(\frac{R_S}{r}\right)^{l+1} \\ & \times\bar{P}_{lm}(\cos\theta_i)\exp(im(\varphi_i-\Omega_{\rm orb}t)) , \end{aligned} \tag{23}$$

using the expansion of the tidal potential of the satellite

$$\begin{aligned} \Phi_{\rm ext} \quad = \quad & \sum_{l,m}\Psi_{lm}\left(\frac{r}{a}\right)^l\bar{P}_{lm}(\cos\theta_i) \\ & \times\exp(im(\varphi_i-\Omega_{\rm orb}t)) , \end{aligned} \tag{24}$$

where the sum is over integers $l\geq 2$ and $-l\leq m\leq l$, θ_i and φ_i are the colatitude and longitude in the inertial frame , and

$$\Psi_{lm}\approx -\frac{Gm_s}{a}\left(\frac{R_S}{a}\right)^l . \tag{25}$$

The pattern speed in the inertial frame, i.e., the azimuthal phase speed, is $\Omega_{\rm orb}$. The Love number, k_{lm}, is usually complex. Dissipative processes lead to $Im(k_{lm})$ that is usually small compared to $Re(k_{lm})$. The imaginary part causes a small phase lag between $\Phi_{\rm nw}$ and $\Phi_{\rm ext}$.

The tidal Love numbers, k_{lm}, depend on the internal structure of Saturn, especially its density distribution. Density profiles increasing toward the center usually produce small Love numbers because the tidal force vanishes at the center of planet. Love numbers also depend on the frequency in the rest frame of Saturn, $m(\Omega_S-\Omega_{\rm orb})$, (e.g. Goodman & Lackner 2009; Ogilvie 2013). Note that the conventionally defined equilibrium tide, (e.g. Goldreich & Nicholson 1989a,b), is frequency independent because it is calculated assuming $\partial/\partial t=0$ so that any time or frequency dependence is erased.

The wave-like part, $\boldsymbol{\xi}_{\rm w}$, is an inertial wave. It does not generate a gravitational potential perturbation in the limit $\sigma<2\Omega_S\ll(GM_S/R_S^3)^{1/2}$, because inertial waves lack the ability to raise a free surface (Ogilvie 2013). According to equations (44) and (46) and discussion below them in Ogilvie (2013), the potential corresponding to the wave-like part is on the order of $\Omega_S^2R_S^3/(GM_S)\Psi_{\rm nw}\sim 0.1\Psi_{\rm nw}$, i.e. about 10 times smaller than that contributed by the non-wave like part. Therefore, if it were an inertial wave attractor that resonantly locks a satellite, the corresponding gravitational perturbation would be nearly the same as that generated by the non-wave like part of the tidal response. Such a small difference would be difficult to distinguish from uncertainties in $\Psi_{\rm nw}$ due to uncertainties in Saturn's interior structure.

5 COMPARISON WITH EXPECTED ACCURACY OF GRAVITY MEASUREMENT BY *CASSINI*

We mentioned at the end of the introduction that *Cassini* will measure the gravitational field of Saturn as it flies by its surface. The anticipated one sigma accuracy for the gravity

[11] We review Ogilvie's result with our own understanding. Readers interested in details are referred to Ogilvie (2013). For general readers, it suffices to read this subsection.

coefficients, J_l, after 6 Proximal orbits are[12],

$$\Delta_2 = 2\times10^{-9}\,, \quad (26)$$
$$\Delta_6 = 2\times10^{-8}\,, \quad (27)$$
$$\Delta_{10} = 1\times10^{-7}\,, \quad (28)$$
$$\Delta_{14} = 2\times10^{-7}\,, \quad (29)$$

given that the gravitational potential of Saturn is expanded as

$$\Phi_S(r>R_S) = -\frac{GM_S}{r}\left[1+\sum_{l=2}^{N_z}\left(\frac{R_S}{r}\right)^l J_l P_{l0}(\cos\theta)\right]\,, \quad (30)$$

where r is the distance from the center of Saturn, P_{lm} are the associated Legendre polynomials[13], and we do not include terms with $m\neq0$ for brevity. We speculate the accuracy declines at high orders J_l because *Cassini* makes gravity measurement mainly at $r\sim2R_S$[14] and the gravitational potential corresponding to higher orders decays faster with distance. Both the potential component associated with J_l and that due to a g mode, Φ_{nl}, declines as $r^{-(l+1)}$. We regard Δ_l as the accuracy of the coefficient associated with the component of the gravitational potential which decays with the $l+1$ power of distance.

Comparing the format of Φ_1 in equation (8) and that of Φ_S in equation (30), we realize that $\Phi_{nl}(r=R_S)$ is associated with $(R_S/r)^l\bar{P}_{l,m=2}(\cos\theta)$, whereas $(-GM_S/R_S)J_l$ is associated with $(R_S/r)^l P_{l,m=0}(\cos\theta)$. We speculate that the accuracy for $\Phi_{nl}(r=R_S)/(-GM_S/R_S)$ is similar to Δ_l. In other words, we speculate the non-axisymmetric component of Saturn's gravitational field due to Saturn's tidal deformations can be measured with similar precision to its axisymmetric gravitational field. We calculate

$$\frac{\Phi_{nl}(r=R_S)}{(-GM_S/R_S)} \sim \frac{\mathcal{B}_{nl}}{n(2l+1)}\left(\frac{r_b}{R_S}\right)^{l+2}\left(\frac{R_S}{a}\right)^2 \times\left(\frac{m_s}{M_S}\right)^{1/2}\left(\frac{\rho_b}{\bar{\rho}}\right)^{1/2}\left(\frac{\dot{a}/a}{(n_r+1)\gamma}\right)^{1/2} \left(\frac{\Omega_S}{\Omega_{\rm orb}}\right)^{3/2}\times\left(\frac{g_S}{g_b}\right)\left(\frac{R_S}{H}\right)^{1/2}\,, \quad (31)$$

Note that $\dot{a}/a$ needs to be replaced by equation (20) for the inner satellite in a MMR. We show an example of the gravity anomaly at the surface of Saturn, $\Phi_{22}(R_S)/(-GM_S/R_S)$, generated by a g mode resonantly locked with Rhea in figure (1). It is above the measurement sensitivity of *Cassini* for most of the range of r_b/R_S.

Linear damping due to turbulent viscosity or heat diffusion yields $\gamma^{-1}\sim(1\sim10)$ Gyr. A gravity mode with azimuthal order $m=2$ has its angular frequency $\sigma=2(\Omega_S-\Omega_{\rm orb})$, within the range for inertial waves, $(-2\Omega_S, 2\Omega_S)$. Therefore, g modes may suffer additional damping upon conversion to inertial waves in the convection zone (e.g. Dintrans & Rieutord 2000; Mathis et al. 2014). Nevertheless, the frequencies of g modes do not generally coincide with frequencies of inertial wave attractors. Considering that inertial waves do not suffer significant damping unless forming an attractor (Ogilvie & Lin 2004; Ogilvie 2013), we speculate that γ does not greatly increase through g mode coupling with inertial waves in the convection zone. There may also exist other damping mechanisms beyond our knowledge. We must acknowledge that γ is very uncertain, and we decide to leave it as a free parameter. Fortunately, $\Phi_{nl}\propto\gamma^{-1/2}$, depending only weakly on γ. The square root dependence can be understood in the following way. The tidal torque on a satellite scales as $T_{\rm osc}\propto\gamma A^2$, while the gravitational potential scales as $\Phi_{nl}\propto A\propto(T/\gamma)^{1/2}$. Since $T\propto\dot{a}/a$, we also have $\Phi_{nl}\propto(\dot{a}/a)^{1/2}$.

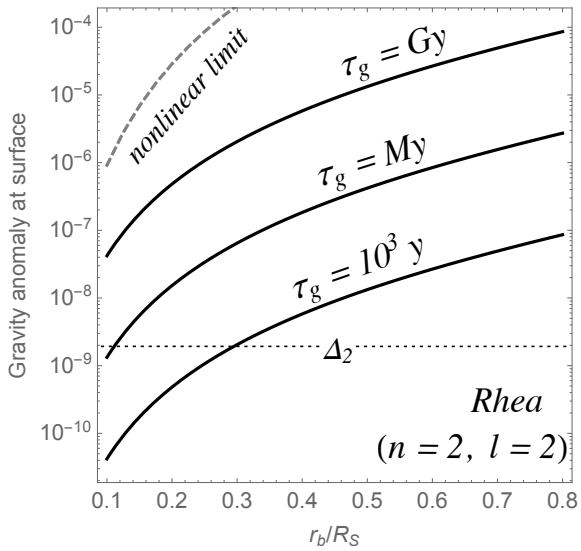

Figure 1. Gravity anomaly at the surface of Saturn, equation (31), for a g mode with $l=2$ and $n=2$ that is resonantly locked with Rhea. The horizontal axis is r_b/R_S, where r_b is the bottom of the outer convection region and the top of the hypothetical stably stratified region. The corresponding mode damping time, τ_g, is labeled beside each curve. The dotted horizontal line shows the measurement sensitivity of *Cassini*. The dashed curve corresponds to $(k_r\xi_r)_{r_b}\sim1$. Nonlinear damping limits the gravity anomaly to lie below this line.

On the other hand, Φ_{nl} depends on r_b/R_S most sensitively. Fuller (2014) propose that $r_b/R_S\approx0.4$ but this value is uncertain. Besides the explicit dependence, $(r_b/R_S)^{(l+2)}$, ρ_b, H and g_b also depend on r_b. For a polytrope with index 1 (Appendix A1), we have $(\rho_b/H/g_b)^{1/2}$ approaches a constant for $r_b/R_S\ll1$. Therefore,

$$\Phi_{nl}\overset{\propto}{\sim}\left(\frac{r_b}{R_S}\right)^{l+2}\,,\ (r_b\ll R_S)\,, \quad (32)$$

yielding that constant Φ_{nl} roughly traces

$$\tau_g\equiv\frac{1}{(n_r+1)\gamma}\propto(r_b/R_S)^{-2l-4}\,,\ (\text{for } r_b\ll R_S)\,. \quad (33)$$

The sensitive dependence of Φ_{nl} on (r_b/R_S) can be understood as follows. The power index l originates from the decaying potential of the lth multipole with distance. The rest of the power index finds its root in the fact that the background density gradient flattens towards small r_b/R_S for a polytrope with index unity. We show right below equation (11) that a flatter density gradient makes it harder for a gravity mode to perturb the gravitational potential.

We illustrate a solid contour line with gravity anomaly

[12] Through private communication with Phillip D. Nicholson.
[13] Not normalized yet.
[14] Private communication with Phillip D. Nicholson.

(equation (31)) equal to Δ_l in figure (2), for Rhea with $l = 2$ and $n = 2,\ 4,\ 6$. The region above each contour line labeled '1' is where the gravity anomaly is greater than Δ_l, where *Cassini* could hopefully detect the gravity potential from a resonantly locked g mode. The limit due to nonlinear effects is above the parameter space shown in this figure.

Gravitational perturbations for other satellites, e.g., Mimas and Enceladus, are similar to figure (2). Note that we only consider $l = 2$ because the measurement accuracy is best at $l = 2$. Assuming Titan also migrates at a rate $\dot{a}/a \sim 1/(5\,\mathrm{Gy})$, it would create a gravity anomaly ~ 10 times larger (at the same r_b/R_S and τ_g) than Rhea.

If inertial wave attractors resonantly lock satellites, then the gravitational potential perturbation is generated by the non-wave-like response of Saturn. The format of Φ_S in equation (30) and Φ_{nw} in equation (23) suggest that we compare Δ_l with

$$\frac{k_{lm}\Psi_{lm}}{(-GM_S/R_S)} \approx k_{lm}\left(\frac{m_s}{M_S}\right)\left(\frac{R_S}{a}\right)^{l+1}. \tag{34}$$

This evaluates to $\approx 2.6 \times 10^{-8} k_{lm}$ for Titan with $l = 2$, which may be detectable. For higher order multipoles and other other satellites, the gravitational perturbations from inertial waves are likely too weak to detect.

The gravitational potential of Saturn is also affected by other types of perturbations, e.g., zonal winds, which may dominate the J_l's. However, the gravitational potential generated by the tidal response of Saturn has its azimuthal phase speed equal to the mean motion of the satellite. Therefore, a frequency analysis can filter out other types of perturbations because they will not follow the same pattern speed as the satellite.

6 FUNDAMENTAL MODES OF SATURN

Hedman & Nicholson (2013) report density waves in the C ring of Saturn that propagate inward. They are believed to be generated by outer Lindblad resonances with fundamental modes (f modes) of Saturn. It is interesting to check whether the f modes are detectable through measuring their gravity anomaly. We estimate the gravitational potential of f modes in an order of magnitude way in appendix D. Additional numerical calculations can be found in Marley & Porco (1993) and Fuller (2014). The $l = m$ component of the perturbed gravitational potential is found to be

$$\frac{\Delta\Phi_f}{(GM_S/R_S)} \sim \frac{2\pi}{m(3m+1)}\left(\frac{r_L}{R_S}\right)^m\left(\frac{\Sigma r_L^2}{M_S}\right). \tag{35}$$

where r_L is the location of the outer Lindblad resonance and Σ is the mass column density at r_L. Estimates of both r_L and Σ are available in tables 4 and 6 in Hedman & Nicholson (2013). We compare the gravity anomaly due to a hypothetical f mode with Δ_m in table 1. Unfortunately, the magnitudes of the gravity anomalies generated by f modes are below the anticipated measurement accuracy of *Cassini*.

The ring system of Saturn is a sensitive seismometer. The discussion above about f modes suggests that Saturn's C ring is an even more sensitive seismometer than *Cassini*. Oscillations of Saturn and gravitational forcing from satellites both excite density waves or bending waves in the ring, as long as their azimuthal phase speed in the inertial frame

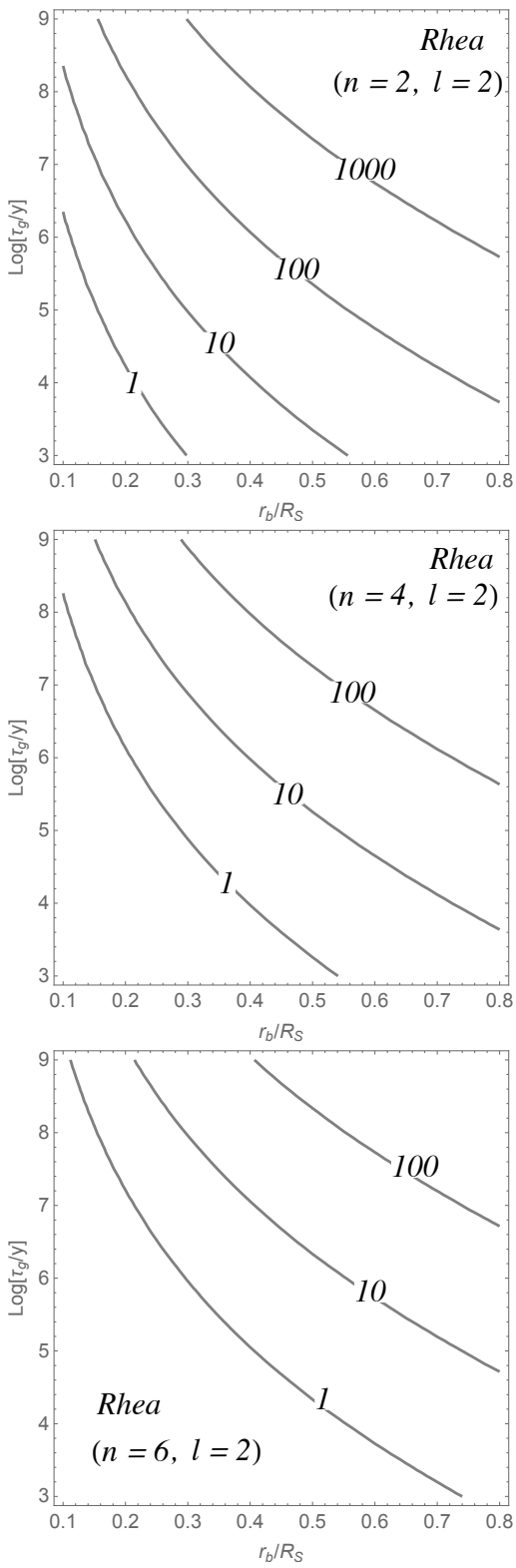

Figure 2. Parameter space in which we compare the gravitational perturbation of a g mode resonantly locked with Rhea with the sensitivity of *Cassini*. The vertical axis is the g mode damping time, $\tau_g \equiv 1/\gamma/(n_r+1)$, in units of years. The solid contour line labeled by '1' shows where the gravity anomaly produced by the resonant g mode, equation (31), is equal to the expected sensitivity of *Cassini*'s gravity measurement, Δ_l. Other solid contour lines show where the gravity anomaly is equal to 10, 100, etc. times Δ_l. The nonlinear limit, $(k_r\xi_r)_{r_b} \sim 1$, lies above the parameter space shown here.

Table 1. Potential perturbation due to f modes at R_S, which is compared with the accuracy of *Cassini*'s gravity measurement, Δ_m. We adopt the same notation for the names of each f mode as those in Hedman & Nicholson (2013). Here Δ_m is the sensitivity for the coefficient associated with the potential component decaying by the $m+1$ power of distance. Given that $\Delta_2 \sim 2\times10^{-9}$ and $\Delta_6 \sim 2\times10^{-8}$ (private communication with Philipp D. Nicholson), we assume that $\Delta_3 \sim \Delta_4 \sim \sqrt{\Delta_2\Delta_6} \sim 6\times10^{-8}$.

Wave	m	r_L (km)	$\Delta\Phi_f/(GM_S/R_S)$	*Cassini* accuracy
W80.98	4	80988	3.1×10^{-10}	6×10^{-8}
W82.00	3	82010	4.0×10^{-10}	6×10^{-8}
W82.06	3	82061	7.1×10^{-10}	6×10^{-8}
W82.21	3	82209	4.9×10^{-10}	6×10^{-8}
W84.64	2	84644	4.8×10^{-10}	2×10^{-9}
W87.19	2	87189	1.9×10^{-10}	2×10^{-9}

matches an integer ratio, p/q, multiplied by the local Keplerian orbital frequency in the ring (e.g. Hedman & Nicholson 2013; Nicholson et al. 2014a,b; French et al. 2016). However, oscillations of Saturn excited by satellites share the same azimuthal phase speed as the satellite, therefore they would produce ring waves at the same location as waves excited directly by the satellite. Unless there is good knowledge about the properties of the rings (e.g. Hedman & Nicholson 2016; Spilker et al. 2004) that precisely constrains the strength of perturbing gravitational potential, the ring system may not distinguish between a tidally excited oscillation of Saturn and the satellite itself.

7 CONCLUSION

Resonance locking between satellites and oscillations of Saturn is a promising mechanism to account for the current surprisingly fast migration of satellites (Lainey et al. 2017). We investigate two channels through which resonance locking can operate. One is to increase the amplitude of an oscillation while keeping the damping rate constant, e.g., a g mode; the other is to increase the damping rate while keeping the amplitude constant, e.g., an inertial wave attractor.

Since the perturbation to the gravitational field of Saturn by an oscillation is proportional to its amplitude, g modes and inertial wave attractors would generate distinctive gravity potentials. The *Cassini* spacecraft will finish its proximal orbits by September 2017. Flying by Saturn closely multiple times, it will constrain the gravity field of Saturn to unprecedented accuracy. According to our estimates, the gravitational potential produced by a g mode resonantly locked with a satellite is detectable for a wide range of the parameter space. Because the azimuthal phase speed of a g mode resonantly locked with a satellite is well known, filtering out the gravity anomaly at the corresponding frequency would largely damp noise due to other reasons, e.g., zonal winds. Additionally, the gravitational perturbation due to a resonantly locked g mode is very sensitive to the depth of the convective region in Saturn. In spite of the uncertain in damping rates of g modes, detection of their gravitational perturbations would provide constraints on the depth of the convective region.

On the other hand, the gravitational perturbations caused by resonantly locked inertial wave attractors are likely too small to detect. However, given the fact that g modes are detectable in a large region of parameter space, a null detection of g modes would favor the operation of inertial wave attractors. The frequencies at which attractors form depend sensitively on the size of the cavity inside which inertial waves are confined. So, the frequencies of inertial wave attractors can also put meaningful constraints on the interior structure of Saturn.

ACKNOWLEDGEMENTS

We thank Peter Goldreich for his insightful suggestions and comments. We thank Phillip D. Nicholson for providing us information about the proximal orbits of *Cassini*. We thank Gordon Ogilvie for his clarification about his work on inertial waves, i.e. Ogilvie (2013). We thank Douglas N C Lin for his comments on inertial wave attractors. This work is supported by the Theoretical Astronomy Center and Center for Integrative Planetary Science at University of California at Berkeley. This research is funded in part by the Gordon and Betty Moore Foundation through Grant GBMF5076 and by the Simons Foundation through a Simons Investigator Award to EQ.

REFERENCES

Barker A. J., Dempsey A. M., Lithwick Y., 2014, ApJ, 791, 13
Borderies N., Goldreich P., Tremaine S., 1982, Nature, 299, 209
Chapman S., Lindzen R., 1970, Atmospheric tides. Thermal and gravitational. D. Reidel Publishing Company, Dordrecht-Holland
Cox J., 1980, The Theory of Stellar Pulsation. Princeton series in astrophysics, Princeton University Press, https://books.google.com/books?id=-kiqQgAACAAJ
Dintrans B., Rieutord M., 2000, A&A, 354, 86
Dunford B., Piazza E., Thompson J. R., 2017, Cassini: the grand finale, https://saturn.jpl.nasa.gov/
Flattery T. W., 1967, Hough functions. University of Chicago. Department of the Geophysical Sciences
French R. G., Nicholson P. D., McGhee-French C. A., Lonergan K., Sepersky T., Hedman M. M., Marouf E. A., Colwell J. E., 2016, Icarus, 274, 131
Fuller J., 2014, Icarus, 242, 283
Fuller J., Luan J., Quataert E., 2016, MNRAS, 458, 3867
Goldreich P., 1965, MNRAS, 130, 159
Goldreich P., Nicholson P. D., 1977, Icarus, 30, 301
Goldreich P., Nicholson P. D., 1989a, ApJ, 342, 1075
Goldreich P., Nicholson P. D., 1989b, ApJ, 342, 1079
Goldreich P., Tremaine S., 1978, ApJ, 222, 850
Goldreich P., Tremaine S., 1982, ARA&A, 20, 249
Goldreich P., Wu Y., 1999, ApJ, 511, 904
Goodman J., Lackner C., 2009, ApJ, 696, 2054
Greenspan H. P., 1958, Journal of fluid Mechanics, 4, 330
Greenspan H., 1968, The Theory of Rotating Fluids. Cambridge Monographs on Mechanics, Cambridge University Press, https://books.google.com/books?id=2R47AAAAIAAJ
Hansen C. J., Kawaler S. D., Trimble V., 2004, Stellar interiors : physical principles, structure, and evolution. Springer
Hedman M. M., Nicholson P. D., 2013, AJ, 146, 12
Hedman M. M., Nicholson P. D., 2016, Icarus, 279, 109
Hodges R., 1967, Journal of Geophysical Research, 72, 3455
Jeffreys H., 1952, The Earth. Cambridge University Press
Lainey V., et al., 2012, ApJ, 752, 14

Lainey V., et al., 2017, Icarus, 281, 286
Longuet-Higgins M. S., 1968, Philosophical Transactions of the Royal Society of London Series A, 262, 511
Luan J., Goldreich P., 2017, AJ, 153, 17
Maas L. R. M., Benielli D., Sommeria J., Lam F.-P. A., 1997, Nature, 388, 557
Marley M. S., Porco C. C., 1993, Icarus, 106, 508
Mathis S., Neiner C., Tran Minh N., 2014, A&A, 565, A47
Murray C. D., Dermott S. F., 1999, Solar system dynamics. Cambridge University Press
Nicholson P. D., French R. G., Hedman M. M., Marouf E. A., Colwell J. E., 2014a, Icarus, 227, 152
Nicholson P. D., French R. G., McGhee-French C. A., Hedman M. M., Marouf E. A., Colwell J. E., Lonergan K., Sepersky T., 2014b, Icarus, 241, 373
Ogilvie G. I., 2013, MNRAS, 429, 613
Ogilvie G. I., Lin D. N. C., 2004, ApJ, 610, 477
Peale S. J., 1999, ARA&A, 37, 533
Pierce J., 1974, Almost All about Waves. MIT Press, https://books.google.com/books?id=tG6bQgAACAAJ
Spilker L. J., Pilorz S., Lane A. L., Nelson R. M., Pollard B., Russell C. T., 2004, Icarus, 171, 372
Urban S., Seidelmann P., 2012, Explanatory Supplement to the Astronomical Almanac. University Science Books, https://books.google.com/books?id=c8pLLwEACAAJ
Weinberg N. N., Arras P., Quataert E., Burkart J., 2012, ApJ, 751, 136
Witte M. G., Savonije G. J., 1999, A&A, 350, 129
Wu Y., Goldreich P., 2001, ApJ, 546, 469

APPENDIX A: LINEAR DAMPING FOR G MODES

A1 Turbulent viscosity

G modes are evanescent in convection zones, and thus the length scale over which the displacement of the mode varies is $R-r_b$, where r_b is the bottom of the convection zone. The energy dissipated per unit time in the convection zone is

$$\dot{E}_{\rm turb} \sim \int_{r_b}^{R} dr\, 4\pi r^2 \rho \nu_{\rm turb} \left(\frac{\dot{\xi}}{R-r_b}\right)^2 , \tag{A1}$$

where the turbulent viscosity is $\nu_{\rm turb} \sim v_l l/3$, with l the size of the convective eddy and v_l its convective velocity. The turnover frequency, v_l/l, must be as fast as the oscillation for the turbulence to act like viscosity. However, the largest scale convective eddies, those as big as the local scale height, turn over very slowly compared to the oscillation frequency, and thus do not act like viscosity. Therefore, we need to consider sub-eddies in the turbulent cascade (Goldreich & Nicholson 1977), which we assume follows a Kolmogorov law, $v_l \propto l^{1/3}$. Thus, setting

$$\frac{v_l}{l} \sim \frac{v_{\rm cv}}{H}\left(\frac{H}{l}\right)^{2/3} , \tag{A2}$$

to σ, we find the sub-eddies that act as viscosity generate

$$\nu_{\rm turb} \sim \frac{1}{3} H v_{\rm cv} \left(\frac{v_{\rm cv}}{H}\frac{1}{\sigma}\right)^2 , \tag{A3}$$

Because $\sigma \gg v_{\rm cv}/H$, the turbulent viscosity is very small. The total energy of a mode with n_r radial nodes is

$$E_{\rm mode} \sim (n_r+1)\int_{r_b}^{R} dr\, 4\pi r^2 \rho \dot{\xi}^2 , \tag{A4}$$

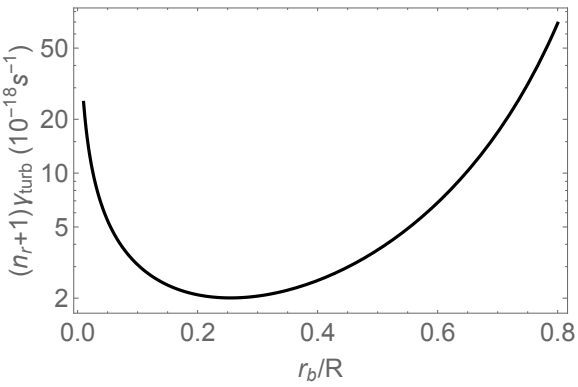

Figure A1.

assuming that the mode energy stored in the evanescent region is the same as that stored between each pair of consecutive radial nodes. Because $\rho\dot{\xi}^2$ decreases outwards in the evanescent zone, the dissipation is dominated by the base of the evanescent zone, i.e.

$$\gamma_{\rm turb} \equiv \frac{\dot{E}_{\rm turb}}{E_{\rm mode}} \sim \frac{1}{(n_r+1)}\frac{1}{(R-r_b)^2}\left(\frac{v_{\rm cv}^3}{\sigma^2 H}\bigg|_{r_b}\right) . \tag{A5}$$

We employ a polytrope of index unity (e.g. Hansen et al. 2004),

$$z = A\,r , \tag{A6}$$

$$\rho(z) = \rho_c \frac{\sin z}{z} , \tag{A7}$$

with

$$A = \frac{\pi}{R_S} \approx 5.4\times 10^{-10}\,{\rm cm}^{-1} , \tag{A8}$$

$$\rho_c = 2.253\,{\rm g\,cm}^{-3} , \tag{A9}$$

where ρ_c is chosen to match Saturn's total mass. Saturn's intrinsic luminosity, $L_{\rm in} \approx 8.45\times 10^{23}\,{\rm erg\,s}^{-1}$, is carried by convection, and it follows that

$$4\pi r^2 \rho v_{\rm cv}^3 = L_{\rm in} . \tag{A10}$$

The scale height is

$$H \sim \left(-\frac{d\ln p}{dr}\right)^{-1} = \left(-2\frac{d\ln\rho}{dr}\right)^{-1} \tag{A11}$$

$$= 2A\left(\cot z - \frac{1}{z}\right) . \tag{A12}$$

It follows that

$$\gamma_{\rm turb} \sim (10^{-18}\sim 10^{-17})\frac{1}{(n_r+1)}\left(\frac{\sigma}{2\Omega_S}\right)^{-2}\,{\rm s}^{-1} \tag{A13}$$

Because $(n_r+1)\gamma$ appears together in the gravitational potential for a g mode (equation 19), we plot $(n_r+1)\gamma_{\rm turb}$ in figure (A1).

Saturn spins quickly compared to its convective turnover frequency, i.e. $2\Omega_S \gg v_{\rm cv}/H$. Therefore, turbulence in Saturn is rotationally altered, since the Coriolis force makes it difficult to convect perpendicular to the spin axis. The major effect of rotation on convection is to make column-shaped eddies with their long axis along the spin axis. However, according to Barker et al. (2014), rotation

hardly affects turbulent viscosity. The derivation of the turbulent viscosity above depends on three conditions: 1, the radial size of eddy is $\sim H$; 2, a Kolmogorov law, equation (A2); 3, the relation between convective velocity and internal luminosity, equation (A10). All three conditions are still satisfied in the simple tank model of Barker et al. (2014). Although rotationally modified convection in Saturn must be more complicated than the tank model, we speculate that rotation mainly modifies the shape of eddies, e.g., the ratio of their radial and horizontal length scales, rather than changing their absolute length scales. The absolute scale of eddies is primarily determined by the internal luminosity.

A2 Damping by heat diffusion

The local thermal timescale of Saturn is

$$\tau_{\rm th} = \frac{4\pi r^2 pH}{L_{\rm in}} \sim 10^{17\sim18}\,{\rm s}\,, \tag{A14}$$

in the deep interior where g modes are likely to propagate. Diffusive processes scale inversely with the square of length, as revealed by the following general formula,

$$\begin{aligned} \rho c_p \frac{\partial T}{\partial t} &= -\boldsymbol{\nabla}\cdot\boldsymbol{F} \\ &= \boldsymbol{\nabla}\cdot(k_{\rm cond}\boldsymbol{\nabla}T)\,, \end{aligned} \tag{A15}$$

where $k_{\rm cond}$ is the effective conductivity. Therefore, the damping rate for g modes by diffusion is

$$\gamma_{\rm diff} \sim \frac{\int dr 4\pi r^2 \rho(\sigma\xi)^2 \frac{(rk_r)^2}{\tau_{\rm th,r}}}{\int dr 4\pi r^2 \rho(\sigma\xi)^2}\,, \tag{A16}$$

where the integration is taken over the whole g mode cavity, and $\tau_{\rm th,r}$ is the thermal timescale at radius r. We observe that $\gamma_{\rm diff}$ is an average of the local diffusive timescale, $(rk_r)^2/\tau_{\rm th,r}$, weighted by the local kinetic energy of the mode. Because the local thermal timescale, $\tau_{\rm th,r} \sim p(r)H(r)/F(r)$, grows rapidly with depth, $\gamma_{\rm diff}$ is dominated by the first half wavelength. Therefore we have

$$\begin{aligned} \gamma_{\rm diff} &\sim \frac{\int_{\lambda_1} dr 4\pi r^2 \rho(\sigma\xi)^2 \frac{(rk_r)^2}{\tau_{\rm th,r}}}{\int dr 4\pi r^2 \rho(\sigma\xi)^2} \\ &\sim \left.\frac{(rk_r)^2}{\tau_{\rm th}}\right|_{r_b} \times \frac{\int_{\lambda_1} dr 4\pi r^2 \rho(\sigma\xi)^2}{\int dr 4\pi r^2 \rho(\sigma\xi)^2} \\ &\sim \left.\frac{(rk_r)^2}{\tau_{\rm th}}\right|_{r_b} \frac{1}{(n_r+1)}\,, \end{aligned} \tag{A17}$$

where in the last line we adopt the fact that the mode energy stored in the first half wavelength is about $1/(n_r+1)$ of the total mode energy. Employing that $k_r \sim (n_r+1)/r$, we derive that

$$\gamma_{\rm diff} \sim \frac{(n_r+1)}{\tau_{\rm th,b}} \tag{A18}$$

$$\sim (10^{-18}\sim10^{-17})(n_r+1)\,{\rm s}^{-1}\,, \tag{A19}$$

which is similar to that due to turbulent viscosity. This derivation of $\gamma_{\rm diff}$ is a standard procedure, and thus we do not list details here. Interested readers are referred to e.g. Goldreich & Wu (1999). Here our intent is to justify that $\gamma_{\rm diff}$ in our case is almost independent of the specific diffusion mechanism, e.g., radiative diffusion, conductivity, etc.

According to the second line of equation (50) of Goldreich & Wu (1999)[15],

$$\gamma_{\rm diff} \propto \int dr \frac{\delta T}{T}\frac{d}{dr}\left(\frac{\delta F}{F}\right)\,, \tag{A20}$$

where the integration is over the whole propagation cavity of a g mode which we assume coincides with the stably stratified region. The only term that the specific diffusion mechanism could affect is $\delta F/F$, because

$$F = -k_{\rm cond}\frac{dT}{dr}\,, \tag{A21}$$

so we obtain

$$\frac{\delta F}{F} = \frac{\delta k_{\rm cond}}{k_{\rm cond}} + \frac{\delta T}{T} - \frac{d\xi_r}{dr} + \left(\frac{d\ln T}{dr}\right)^{-1}\frac{d}{dr}\left(\frac{\delta T}{T}\right)\,, \tag{A22}$$

where $\delta k_{\rm cond}/k_{\rm cond}$ creates dependence on the specific diffusion mechanism. However, in the propagation cavity of a g mode, $k_r > 1/H$, where $1/H$ is the scale over which the unperturbed quantities vary. Therefore, terms containing a gradient of perturbed quantities, namely the last two terms in equation (A22), dominate $\delta F/F$. Approximately,

$$\frac{\delta F}{F} \approx -\frac{d\xi_r}{dr} + \left(\frac{d\ln T}{dr}\right)^{-1}\frac{d}{dr}\left(\frac{\delta T}{T}\right)\,. \tag{A23}$$

It follows that $\delta F/F$ is approximately independent of $k_{\rm cond}$, as is $\gamma_{\rm diff}$.

APPENDIX B: EULERIAN DENSITY PERTURBATION

Because we are interested in the first half wavelength, we can adopt a plane-parallel model with constant gravity, g. Then equation (7) of Goldreich & Wu (1999) applies, which we copy below,

$$\xi_z = \frac{-g\sigma^2}{(gk_h)^2-\sigma^4}\left[\frac{p}{\rho g}\frac{d}{dz}\left(\frac{\delta p}{p}\right) + \left(1-\frac{k_h^2 p}{\sigma^2\rho}\right)\left(\frac{\delta p}{p}\right)\right]\,, \tag{B1}$$

where z is the vertical depth that increases downward, i.e., in the same direction of gravity, g. Here, δ denotes a Lagrangian perturbation. Note that this expression is general, without assuming $\nabla\cdot\xi = 0$ or $\delta\rho/\rho = 0$. We can neglect the σ^4 in the denominator because $\sigma^2 \ll gk_h$ for a g mode in Saturn. For an adiabatic perturbation, $\delta\rho/\rho = \delta p/p/\Gamma_1$, and we have

$$\frac{\rho'}{\rho} = \frac{1}{\Gamma_1}\frac{\delta p}{p} - \xi_z\frac{d\ln\rho}{dz} \tag{B2}$$

$$\approx \left(\frac{1}{\Gamma_1} - \frac{d\ln\rho}{d\ln p}\right)\frac{\delta p}{p} + \frac{\sigma^2}{gk_h}\frac{d\ln\rho}{dz}\frac{1}{k_h}\frac{\delta p}{p} \tag{B3}$$

$$+\left(\frac{d\ln\rho}{d\ln p}\right)\frac{\sigma^2}{gk_h}\frac{1}{k_h}\frac{d}{dz}\left(\frac{\delta p}{p}\right)\,. \tag{B4}$$

In the absence of a molecular weight gradient,

$$N^2 = -g\left(\frac{1}{\Gamma_1}\frac{d\ln p}{dz} - \frac{d\ln\rho}{dz}\right)\,, \tag{B5}$$

[15] Entropy diffusion along horizontal direction is neglected, which is a good approximation for g mode, because $k_r \gg k_h$.

which may not be true but will not affect the generality of our discussion. Then we obtain

$$\frac{\rho'}{\rho} \approx -\frac{N^2}{g} H_p \left(\frac{\delta p}{p}\right) + \frac{\sigma^2}{gk_h} \frac{d\ln\rho}{dz} \frac{1}{k_h} \left(\frac{\delta p}{p}\right) + \left(\frac{d\ln\rho}{d\ln p}\right) \frac{\sigma^2}{gk_h} \frac{1}{k_h} \frac{d}{dz} \left(\frac{\delta p}{p}\right) . \quad \text{(B6)}$$

In the first half wavelength, λ_1, at the top of the propagation cavity we have the following approximations,

$$k_z \sim k_h \frac{N}{\sigma} , \quad \text{(B7)}$$

$$k_z \sim \frac{1}{\lambda_1} \sim \frac{1}{H} , \quad \text{(B8)}$$

$$H \sim H_p \sim H_\rho , \quad \text{(B9)}$$

where $H_\rho \equiv dz/d\ln\rho$ is the density scale height, and we do not distinguish it from the pressure scale height, $H_p \equiv dz/d\ln p = p/(\rho g)$, and we label both of them by H. Adopting these approximations, we realize that the three terms in equation (B6) are of the same order of magnitude. For convenience, we choose the second term to represent ρ'/ρ, i.e.,

$$\frac{\rho'}{\rho} \sim \left(\frac{\sigma^2}{gk_h}\right) \frac{d\ln\rho}{dz} \frac{1}{k_h} \left(\frac{\delta p}{p}\right) . \quad \text{(B10)}$$

Next, let us relate ρ'/ρ to ξ_z. For Saturn, if we use a polytrope with index unity, we note that $k_h^2 p/(\rho\sigma^2) \gg 1$. In the first half wavelength, $p/(\rho g) = H_p \sim H$, $d(\delta p/p)/dz \sim -(\delta p/p)/\lambda_1$ and $H \sim \lambda_1$. It follows that the first two terms in ξ_z, equation (B1), are similar to each other and both are much smaller than the third term. Therefore, we obtain,

$$\xi_z \sim H \left(\frac{\delta p}{p}\right) . \quad \text{(B11)}$$

Combining equations (B10) and (B11), we obtain

$$\rho' \sim \frac{d\rho}{dz} \xi_z \frac{\sigma^2 \rho}{k_h^2 p} \sim \frac{d\rho}{dr} \xi_r \frac{\sigma^2 \rho}{k_h^2 p} , \quad \text{(B12)}$$

where we have changed the coordinate from z to r.

APPENDIX C: THE FIRST HALF WAVELENGTH DOMINATES THE GRAVITY POTENTIAL OF G MODE

We consider a simple Brunt-Vaisala frequency profile, i.e. $N = N_0$ between $r_c < r < r_b$. The number of radial nodes is

$$\pi n_r \sim \int_{r_c}^{r_b} dr\, k_r \sim \int_{r_c}^{r_b} dr\, \frac{K_n^{1/2}}{r} \frac{N_0}{\sigma} \sim K_n^{1/2} \frac{N_0}{\sigma} \ln\left(\frac{r_b}{r_c}\right) . \quad \text{(C1)}$$

Similarly the $\tilde{n}$th node satisfies

$$\pi\tilde{n} \sim K_n^{1/2} \frac{N_0}{\sigma} \ln\left(\frac{r_b}{r_{\tilde{n}}}\right) . \quad \text{(C2)}$$

which means that the $\tilde{n}$th node is at a radius,

$$r_{\tilde{n}} = r_b \left(\frac{r_c}{r_b}\right)^{\tilde{n}/n_r} , \ (\tilde{n} = 0, 1, \ldots, n_r - 1). \quad \text{(C3)}$$

The radial wavelength at the $\tilde{n}$th node is

$$\lambda_{\tilde{n}} \sim \left.\frac{1}{k_r}\right|_{r_{\tilde{n}}} \sim \left(\frac{r}{K_n^{1/2}} \frac{\sigma}{N_0}\right)_{r_{\tilde{n}}} \sim \frac{r_{\tilde{n}}}{\pi n_r} \ln\left(\frac{r_b}{r_c}\right) . \quad \text{(C4)}$$

The mode energy in each half wavelength is the same, and we express it in the $\tilde{n}$th half wavelength,

$$E_{\rm node} \sim \left(r^2 \rho\lambda(\sigma\xi_h)^2\right)_{r_{\tilde{n}}} \sim \left(r^2 \lambda\rho N_0^2 \xi_r^2\right)_{r_{\tilde{n}}} , \quad \text{(C5)}$$

yielding

$$\xi_{r,\tilde{n}} \sim (-1)^{\tilde{n}-1} E_{\rm node}^{1/2} \left(\frac{\pi\, n_r}{\ln(r_b/r_c)}\right)^{1/2} \frac{1}{N_0} \left(\frac{1}{r^{3/2}} \frac{1}{\rho^{1/2}}\right)_{r_{\tilde{n}}} . \quad \text{(C6)}$$

Note that ξ_r switches sign in consecutive half wavelengths. We assume that ξ_r is positive in the first half wavelength, which is an arbitrary assumption. Then it follows that

$$\Sigma_{\tilde{n}} \approx \left.\frac{d\rho}{dr}\right|_{\tilde{n}} \xi_{r,\tilde{n}} \frac{\sigma^2}{gk_h} \lambda_{\tilde{n}} \approx (-1)^{\tilde{n}} E_{\rm node}^{1/2} \frac{\sigma^2}{gk_h} \left(\frac{\ln(r_b/r_c)}{\pi\, n_r}\right)^{1/2} \frac{1}{N_0} \left(\frac{1}{r^{1/2}} \frac{d\rho^{1/2}}{dr}\right)_{r_{\tilde{n}}} . \quad \text{(C7)}$$

According to equation (9), the $\tilde{n}$th half wavelength contributes a gravitational potential perturbation,

$$\Phi_{\tilde{n},\,nl}(r > r_{\tilde{n}}) = -4\pi G \Sigma_{\tilde{n}} r_{\tilde{n}} \frac{\mathcal{B}_{nl}}{(2l+1)} \left(\frac{r_{\tilde{n}}}{r}\right)^{l+1} \quad \text{(C8)}$$

$$\sim (-1)^{\tilde{n}-1} \frac{2\pi^{1/2}\mathcal{B}_{nl}}{(2l+1)} G \frac{E_{\rm node}^{1/2}}{N_0} \left(\frac{\ln(r_b/r_c)}{n_r}\right)^{1/2} \times \left.\frac{d\rho^{1/2}}{dr^{1/2}}\right|_{r_{\tilde{n}}} \left(\frac{r_{\tilde{n}}}{r}\right)^{l+1} \left(\frac{\sigma^2}{gk_h}\right)_{\tilde{n}} \quad \text{(C9)}$$

$$\sim (-1)^{\tilde{n}-1} \frac{2\pi\mathcal{B}_{nl} G E_{\rm node}^{1/2}}{(2l+1) K_n^{1/4}} \frac{\sigma^{1/2}}{N_0^{3/2}} \left(\frac{r_b}{r}\right)^{l+1} \times \left(\frac{d\rho^{1/2}}{dr^{1/2}}\right)_{r_{\tilde{n}}} \left(\frac{r_c}{r_b}\right)^{\frac{\tilde{n}}{n_r}(l+1)} \left(\frac{\sigma^2}{gk_h}\right)_{\tilde{n}} \quad \text{(C10)}$$

Note that gk_h approaches a constant for $r_b/R_S \ll 1$. We consider two cases of $d\rho^{1/2}/dr^{1/2}$. First, let us assume it is constant. Then

$$\Phi_{nl,\rm tot} = \sum_{\tilde{n}=0}^{n_r-1} \Phi_{\tilde{n},\,nl}(r > R) \quad \text{(C11)}$$

$$\sim \Phi_{\tilde{n}=0,\,nl}(r > R) \left(1 + \left(\frac{r_c}{r_b}\right)^{\frac{(l+1)}{n_r}}\right)^{-1} \quad \text{(C12)}$$

For a polytrope with index unity, $\rho = \rho_b \sin z/z$, where $z = \pi r/R$, and

$$\frac{d\rho^{1/2}}{dr^{1/2}} = -\frac{\rho_b^{1/2}}{3} \left(\frac{\pi}{R}\right)^2 r^{3/2} . \quad \text{(C13)}$$

It follows that

$$\Phi_{nl,\rm tot} = \sum_{\tilde{n}=0}^{n_r-1} \Phi_{\tilde{n},\,nl}(r > R) \quad \text{(C14)}$$

$$\sim \Phi_{\tilde{n}=0,\,nl}(r > R) \left(1 + \left(\frac{r_c}{r_b}\right)^{\frac{(l+5/2)}{n_r}}\right)^{-1} \quad \text{(C15)}$$

In both cases, the outermost ($\tilde{n} = 0$) half wavelength dominates the total $\Phi_{nl\,\rm tot}$, and the combined effect of all other

half wavelengths is to reduce the contribution from the first half wavelength by a factor of two, at most.

APPENDIX D: POTENTIAL OF F MODES EXCITING DENSITY WAVES IN C RING

We assume the potential perturbation of an f mode outside Saturn to have spatial dependence

$$\Phi_f = \Delta\Phi_f \left(\frac{R_S}{r}\right)^{l+1} \bar{P}_{lm}(\cos\theta_I)\cos(m\varphi_I - \sigma t) \quad \text{(D1)}$$

$$\sim \Delta\Phi_f \left(\frac{R_S}{r}\right)^{m+1} \cos(m\varphi_I - \sigma t)\,. \quad \text{(D2)}$$

where θ_I and φ_I are the colatitude and longitude measured in the inertial frame. We set $\theta_I = \pi/2$ because the C ring lies in the equatorial plane of Saturn. We consider the case $l = m$, which, for a given m, induces the strongest perturbation in the C ring. It excites a density wave at an outer Lindblad resonance (Hedman & Nicholson 2013). Thus its pattern speed, i.e., the azimuthal phase speed, $\dot{\varphi}_I = \sigma/m$, satisfies

$$\frac{\sigma}{m} = \frac{m+1}{m}\Omega_{\rm orb}(r_L)\,, \quad \text{(D3)}$$

at the outer Lindblad resonance radius, r_L. Here m is a positive integer, but note that Hedman & Nicholson (2013) denote a negative azimuthal order for an outer Lindblad resonance. We express r and φ_I in terms of osculating elements of a ring particle's orbit to the first order of eccentricity (Murray & Dermott 1999),

$$r \approx a(1 - e\cos\lambda)\,, \quad \text{(D4)}$$

$$\varphi_I \approx \lambda + \varpi + 2e\sin\lambda\,, \quad \text{(D5)}$$

where λ is the mean longitude with revolution rate $\dot{\lambda} = n(a)$, ϖ is the longitude of pericenter, a is the semi-major axis, and e is eccentricity. We submit these expressions into Φ_f and retain the term slowly varying with time,

$$\Phi_{f,s} \sim \frac{3m+1}{2}\left(\frac{R}{a}\right)^{m+1} \Delta\Phi_f e\cos\phi\,, \quad \text{(D6)}$$

where s denotes 'slow', and $\phi \equiv (m+1)\lambda - \sigma t + m\varpi$. Since $\sigma = (m+1)n(r_L)$, and $\dot{\lambda} = \Omega_{\rm orb}(r)$, and ϖ changes slowly with time, this term varies slowly with time near $r = r_L$ and it dominates the secular perturbation to the ring. This perturbing potential pumps eccentricity at a rate (Goldreich & Tremaine 1982),

$$\frac{de}{dt} = \frac{1}{na^2 e}\frac{\partial\Phi_{f,s}}{\partial\varpi} \quad \text{(D7)}$$

$$\sim -n\frac{m(3m+1)}{2}\left(\frac{R_S}{a}\right)^m \frac{\Delta\Phi_f}{(GM_S/R_S)}\sin\phi\,, \quad \text{(D8)}$$

which is maximized if $\phi = \pi/2$ or $3\pi/2$.

The dispersion relation for density waves in a self-gravitating disk in which pressure is negligible (Goldreich & Tremaine 1978) is

$$(\sigma - m\Omega_{\rm orb}(r))^2 = \kappa(r)^2 - 2\pi G\Sigma|k|\,, \quad \text{(D9)}$$

where $\kappa(r)$ is the epicyclic frequency and is $\approx \Omega_{\rm orb}(r)$, Σ is the mass surface density, and k is the wave number. Near the outer Lindblad resonance, we have

$$|k| \sim \frac{m+1}{G\Sigma}\left.\frac{dn^2}{dr}\right|_{r_L}(r - r_L) \sim \frac{(m+1)}{\Sigma}\frac{M_S}{r_L^4}(r_L - r)\,, \quad \text{(D10)}$$

which requires $r < r_L$, i.e., the density wave generated at the outer Lindblad resonance propagates inward. The first half wavelength is given by

$$\pi = \int_{r_L-\lambda_1}^{r_L} |k|dr\,, \quad \text{(D11)}$$

yielding

$$\lambda_1 \sim \frac{r_L}{(m+1)^{1/2}}\left(\frac{\Sigma r_L^2}{M_S}\right)^{1/2}\,. \quad \text{(D12)}$$

The group velocity is

$$v_g = \frac{\partial\sigma}{\partial k} \sim -\frac{\pi G\Sigma}{n}\,. \quad \text{(D13)}$$

The duration of the perturbing potential being in phase with the particle's epicyclic motion is

$$t_{\rm coh} \sim \frac{\lambda_1}{v_g} \sim \frac{1}{n}\frac{1}{\pi(m+1)^{1/2}}\left(\frac{M_S}{\Sigma r_L^2}\right)^{1/2}\,. \quad \text{(D14)}$$

Therefore, the eccentricity changes by

$$\Delta e \sim \frac{de}{dt}t_{\rm coh} \quad \text{(D15)}$$

$$\sim \frac{\Delta\Phi_f}{(GM_S/R_S)}\left(\frac{M}{\Sigma r_L^2}\right)^{1/2}\left(\frac{R_S}{r_L}\right)^m \frac{m(3m+1)}{2\pi(m+1)^{1/2}}\,. \quad \text{(D16)}$$

In order to generate a significant density variation, the excited epicyclic motion needs to cause orbits of different particles to almost cross. Borderies et al. (1982) derive the following criterion using a streamline model, i.e.,

$$q \sim \left(\frac{de}{d\ln a}\right)^2\,. \quad \text{(D17)}$$

needs to be a good fraction of unity[16]. In our case,

$$q \sim \left(a\frac{\Delta e}{\lambda_1}\right)^2\,. \quad \text{(D18)}$$

Equating q to unity leads to

$$\frac{\Delta\Phi_f}{(GM_S/R_S)} \sim \frac{2\pi}{m(3m+1)}\left(\frac{r_L}{R_S}\right)^m\left(\frac{\Sigma r_L^2}{M_S}\right)\,, \quad \text{(D19)}$$

where we have replaced a by the outer Lindblad radius, r_L. We calculate the value of equation D19 using the density waves in the C ring reported by Hedman & Nicholson (2013), by adopting the surface density in their table 6 and the resonant location in their table 4. We list the corresponding potential perturbations due to f modes in table (1). We show that they are below the anticipated sensitivity of the gravity measurement of *Cassini*.

This paper has been typeset from a TEX/LATEX file prepared by the author.

[16] There is a second term in the definition of q in Borderies et al. (1982) describing the 'twisting' effect as the longitude of pericenters change with a. This term is similar to the first term, $(de/d\ln a)^2$, in the first half wavelength, and therefore for our order-of-magnitude estimate we only estimate the first term.